Received: 6 October 2021 | Accepted: 9 January 2022

DOI: 10.1002/maco.202112839

ARTICLE

Materials and Corrosion

Transient and gradient analyses of depolarization criteria. Valuable tools in chloride-induced rebar corrosion monitoring

Christoph Zausinger | **Kai Osterminski** | **Christoph Gehlen**

Department of Materials Engineering, Centre for Building Materials, Chair of Materials Science and Testing, School of Engineering and Design, Technical University of Munich, Munich, Germany

Correspondence
Christoph Zausinger, Department of Materials Engineering, Centre for Building Materials, Chair of Materials Science and Testing, School of Engineering and Design, Technical University Munich, Munich 80333, Germany.
Email: christoph.zausinger@tum.de

Funding information
Bundesministerium für Wirtschaft und Energie, Grant/Award Number: 03TNH025B

Abstract

The aim of this study is to elucidate suitable methods of corrosion monitoring for chloride-induced rebar corrosion in cracked concrete. Depolarization gradients and transients provide evidence for the electrode kinetics at the steel–concrete interface and the geometry of the macrocell. In the present study, a set of cracked, short-term chloride-exposed, reinforced concrete specimens is investigated in terms of their corrosion activity. Primarily, the depolarization behavior was observed by short-term high-frequency measurements, allowing for cost-effective measurement campaigns and robust results. All measurement intervals are split apart via a gradient analysis to enable a congruent, numerical transient analysis. Since the geometry of macrocells in rebar corrosion follows the model of a series of ohmic resistances with a parallel connection of a diffusion-controlled capacitor and an ohmic resistance, the transient of each depolarization curve with unit time in seconds provides evidence for the present electrode kinetics and macrocell geometry. According to the time, which is consumed until a certain state of depolarization is reached, transient modeling can be used to predict corrosion activity as a function of chloride ingress.

KEYWORDS

chloride-induced corrosion, cracked concrete, depolarization, transient analysis

1 | INTRODUCTION

1.1 | State of knowledge

For many decades, massive construction has relied on the application of reinforced concrete as a composite material. As long as the alkalinity of the concrete pore solution exists, the present reinforcement is protected against corrosion. However, once the alkalinity is lost via, for example, chloride ingress along cracks, corrosion can set in, causing latent, local loss of rebar cross section, and results in a significantly shortened service life. Hence, monitoring of rebar corrosion is becoming increasingly important, and adaptable methods to quantify the ongoing corrosion are key factors.

Numerical analysis of polarization behavior of rebar corrosion in concrete is known to be one of the most important approaches to predict corrosion activity.[1,2] Numerical studies have been performed on alternating cell geometries and electrode surface ratios,[3] temperature dependencies,[4] and cracked concrete.[5,6] Transient analysis of open circuit potentials has been reported by Issacs and

Cho,[7] and transient analysis of potential and current decay constants has been conducted by Birbilis and Holloway.[8,9] Most of the studies on corrosion monitoring have the clear goal of quantifying the true loss of cross section due to galvanic loss of mass. Even though many studies yielded a reliable threshold value for a current density of 1 $\mu A\,cm^{-2}$,[10] the method of quantification of the effective surface area is still highly debated. This uncertainty is still a major issue in corrosion quantification and in the assessment of the effectivity of several repair methods.[11] The present study could possibly provide a valuable concept to quantify the effective surface.

A concept of corrosion monitoring needs applicability in real reinforced concrete structures as well as reliable and reproducible methods to determine the corrosion activity at any given time. Once the three-electrode corrosion sensor is installed like in studies of,[12] whether on-site or in the laboratory, the combined measurement of corrosion current and transient analysis of depolarization curves yields such a desired concept. The detection of potential transition from closed to open circuit potential provides plenty of valuable information. This information allows a much better understanding of the macrocell surface and the evolution of the macrocell surface at the time of observation. The exact specimen setup and the formulas that are used for the numerical analysis in the present study are discussed in the following sections.

1.2 | Physical background

In terms of control technology, corrosion of steel in reinforced concrete can be considered as a rather simple equivalent circuit diagram like the Randles circuit (compare Figure 1).[13]

The design of this equivalent circuit diagram neglects intentionally the diffusion-controlling features. More complex features like Warburg elements are viable but expedient in this case. As the goal of this study is to elucidate the relationship between surface kinetics and depolarization time constants, a closer look at the influence of diffusion within the galvanic cell is the topic of future research.

Here, the ohmic, electrolytic resistance (R_E) is solely in series with a parallel connection of two double-layer capacitors ($C_{DL,A}$, $C_{DL,C}$) and two ohmic charge-transfer resistances ($R_{CT,A}$ and $R_{CT,C}$). The indices A and C describe the affiliation of each to either the anode or the cathode. As long as the switch is closed, macrocell corrosion is active and both capacitors are carrying charges, according to the maximum redox driving potential ΔE. Moreover, the capacity of each double-layer capacitor correlates directly to the present electrode surface. Due to changes in environmental conditions, the active surface can change over time and needs to be determined, to enable quantitative corrosion monitoring.

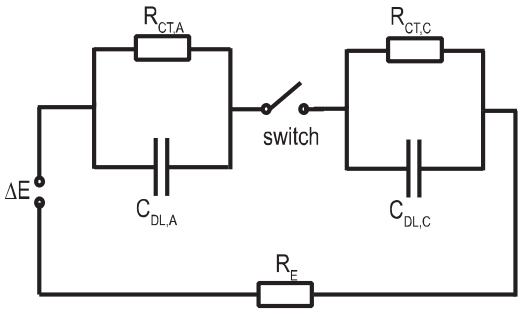

FIGURE 1 Equivalent circuit diagram of the present macrocell with a switchable state from open to closed circuit and vice versa

As soon as the circuit is opened, current flow immediately stops abruptly, a part of the driving potential drops (IR-drop) on the electrolytic resistance (R_E) according to the present ionic conductivity of the concrete, and finally, the remaining cathodic and anodic potentials increase and decrease, respectively. As charge can no longer transfer along the capacitors, both capacitors charge exponentially with time (Equations (1) and (2)).

$$E_{t,A} = E_{corr,A} \cdot e^{-\left(\frac{1}{RC_A}\right)\cdot t} + E_{t30,A}, \tag{1}$$

$$E_{t,C} = E_{corr,C} \cdot \left(1 - e^{-\left(\frac{1}{RC_C}\right)\cdot t}\right) + E_{t30,C}. \tag{2}$$

The exponential charge with time can be analyzed numerically by fitting the depolarization curves of both electrodes. As the starting potential $E_{corr,j}$, depolarization time t, and customized final potential $E_{t30,j}$ (with $j = \{A;C\}$) were measured, the transients RC_A and RC_C are the only remaining variables. This variable RC_j provides an indication of electrode kinetics in terms of the charge-transfer resistance indicated by R as well as the relative change of capacity indicated by C. As R and C will not be treated individually, the variable will be depicted as RC. If, for example, the anodic surface area increases equivalently to the anodic capacitance with, for example, increasing chloride ingress, the anodic transient will decrease. If the cathodic surface area increases equivalently to the cathodic capacitance, for example, with increasing supplementation of oxygen and water, the cathodic transient will decrease. Thus, the RC transient of each electrode is a measure in seconds of corrosion favoring or limiting environments, whereby the active electrode surface is implemented.

TABLE 1 Concrete composition, reinforcement, and crack details

Category	Parameter
Cement type	CEM I 42,5 R
Grading curve	A/B 8
w/b	0.55
Cement ratio	350 kg m^{-3}
Concrete cover anode	35 mm
Concrete cover cathode	40 mm
Steel rebar	10 mm Ø, B500B
Glass fiber rebar	Schöck-Combar® 8 mm Ø
Crack	Transverse, parallel to rebar, width 0.3 mm

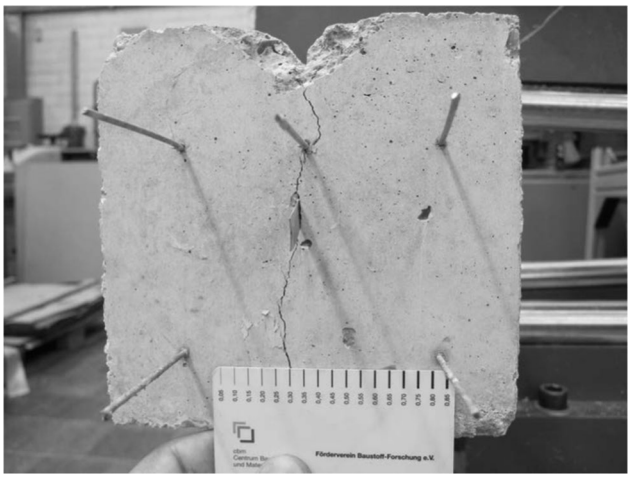

FIGURE 2 Cross section of the reinforced concrete specimen with four cathodic steel rebars and one anodic steel rebar in the upper center of the crack

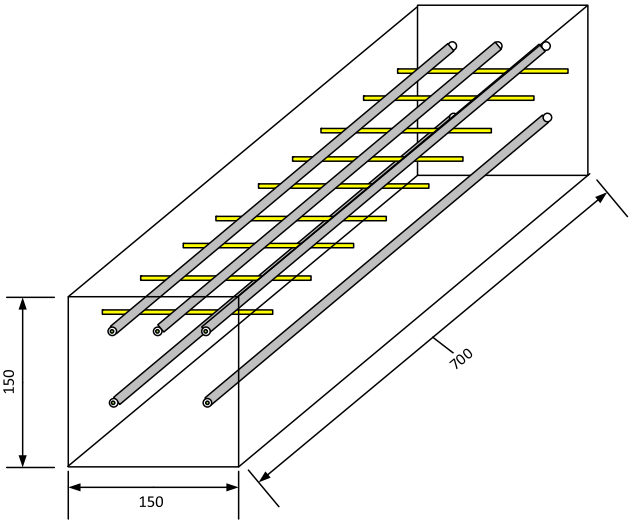

FIGURE 3 3D-sketch of the reinforced concrete specimens with dimensions in millimeters. Five reinforcement steel electrodes and nine glass fiber rebars [Color figure can be viewed at wileyonlinelibrary.com]

2 | METHODS

A set of 12 reinforced, short-term chloride-exposed, cracked concrete specimens was used to enable investigations on corrosion mechanisms in analogy to real, frequented reinforced concrete structures. In the present study, the assessment focuses on electrochemical parameters and their correlation during and after chloride penetration.

The electrical contact and accurate positioning of the investigated steel rebar were ensured within metric formworks. To complete the three-electrode setup, a MnO_2-reference electrode was positioned in the center of the specimen below the anodic rebar before concreting. On the one hand, the previously defined position of each reference electrode accepts the distance to a probably distanced formation of an anode, but on the other hand, a very little IR-Drop between the anode and the reference electrode is ensured.

A summary of the characteristics of the investigated reinforced concrete specimens is shown in Table 1.

In this study, the water to binder ratio was set very high, as most of the real reinforced concrete structures with corrosion activity have high porosity. The porosity, including inhomogeneity at the steel–concrete interface, is one of the most important factors in corrosion mechanisms.[14]

After 28 days of posttreatment with a regularly wetted concrete surface, the specimens were stored at 65% rel. hum. and 20°C. The transverse crack was initiated by a symmetric reduction of cross section along the desired crack position, and the orthogonally oriented glass fiber rebar ensured crack fixation (compare Figures 2 and 3). Perpendicular to the reduction edges, a compressive pressure was applied until the crack formation reached the desired width of 0.3 mm. As soon as crack formation was complete, the specimens were sealed circumferentially using an aluminum laminated butyl rubber tape. The anodic steel bar was centered in the crack and two pairs of identical steel, serving as the cathode, were laterally arranged at distances of 35 and 74 mm, respectively.

The electrical contact of each rebar electrode occurred outside of the sample at the front welded noble steel pins (compare Figure 2).

With the first contamination of a 1.5% chloride solution in the crack, corrosion was initiated, and the corrosion current as well as the corrosion potential were

logged each hour. The current was measured between the working electrode and the counter electrode; the potential was measured against the reference electrode. The reference factory settings were calibrated with 250 mV versus Ag/AgCl. The duration of chloride contamination lasted 3 months, and was followed by 3 months of post-contamination observation. Additionally, a depolarization measurement with a set of two Gamry Interface 1000 (input resistor $>10^{12}\,\Omega$) at 100 Hz for 30 s was performed every month to gain better insight into the electrochemical processes occurring at the steel–concrete interface. The depolarization measurement was performed synchronously at both the working and counter electrodes; both the working and counter electrodes shared the same reference electrode arising from the three-electrode setup described above. For the first 2–3 s of measurement, the circuit was kept closed, and then the circuit was opened manually and the depolarizing potential was measured for the remaining time of about 28 s. Thus, the observation and analysis of the closed circuit potential, the IR-drop, and the transient open circuit potential can be performed in a simple manner, but very precisely.

3 | RESULTS AND DISCUSSIONS

3.1 | Discretization of depolarization curves

For the sake of clarity, the gradient analysis will be described only for the anodic depolarization curves. Except for switched signs, the cathode analysis follows the same criteria.

As mentioned earlier, each depolarization curve consists out of three measurement intervals (compare Figure 4):

- Closed circuit potential
- IR-drop
- Transient open circuit potential

The corrosion potential is a straightforward measure, whereas the IR-drop and transient depolarization must be specified numerically. A gradient analysis of the time interval including the IR-drop allows for an extraction of the potential drop by a numerical tool (compare Figure 5).

As the derivation of the measured, anodic potential-time function shows a sharp negative parable around the IR-drop, a customized criterion needs to be defined, for which the derivation dE/dt in Vs^{-1} can be exclusively assigned to the IR-drop. As soon as the criterion (here $-0.03\ \mathrm{Vs}^{-1}$) is validated graphically, the integration of the dE/dt curve gives the appropriate value of IR-drop due to potential loss in the electrolyte (Equation 3).

$$E_{\mathrm{IR,A}} = \int_0^t \frac{dE}{dt}dt \text{ for } \frac{dE}{dt} < -0.03\mathrm{Vs}^{-1} \tag{3}$$

$$E_{\mathrm{IR,C}} = \int_0^t \frac{dE}{dt}dt \text{ for } > 0.03\mathrm{Vs}^{-1} \tag{4}$$

The IR-drop was determined at low values between 5 and 15 mV on the cathodic site and between 5 and 55 mV on the anodic site, which confirmed the measurement setup described at the beginning of this article.

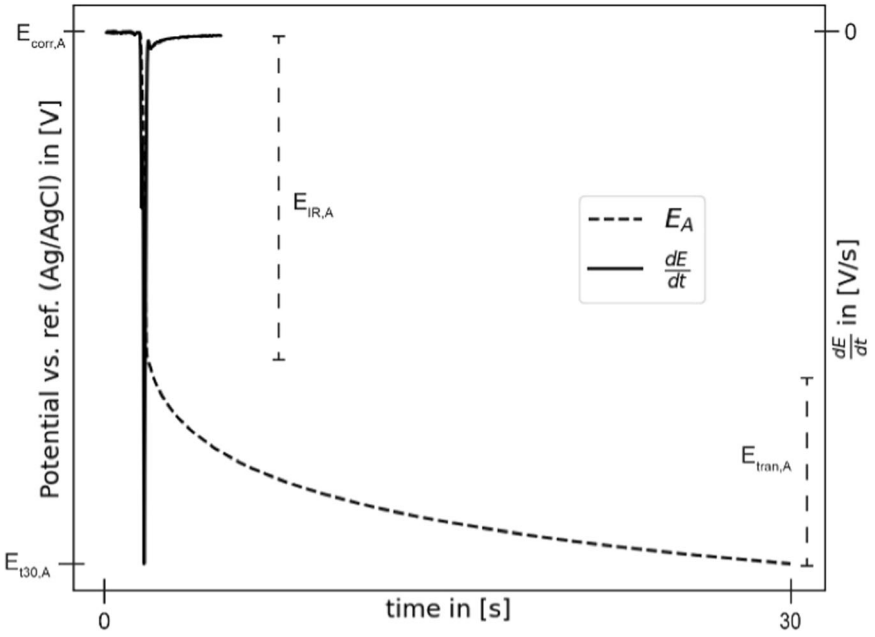

FIGURE 4 Discretization of depolarization intervals into corrosion potential $E_{\mathrm{corr,A}}$, IR-drop $E_{\mathrm{IR,A}}$, and transient potential $E_{\mathrm{tran,A}}$

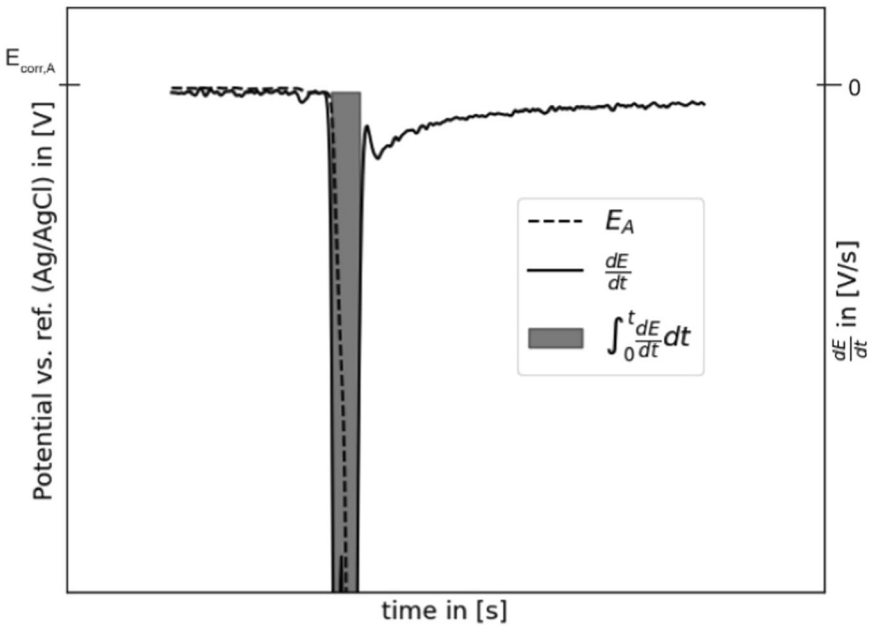

FIGURE 5 Enlarged section of the gradient analysis at the beginning of the IR-drop. The shaded area corresponds to the value of the potential that is lost in the electrolyte

The product of potential loss in the electrolyte between both electrodes and the measured cell current yields the electrolytic resistance. According to Osterminski,[15,16] the remaining two system resistances $R_{CT,A}$ and $R_{CT,C}$ can then be calculated as well:

$$R_E = \frac{E_{IR}}{I_{corr}}, \tag{5}$$

$$R_{CT,A} = \frac{E_{corr,A} - E_{t30,A} - E_{IR,A}}{I_{corr}}, \tag{6}$$

$$R_{CT,C} = \frac{E_{t30,C} - E_{corr,C} - E_{IR,C}}{I_{corr}}. \tag{7}$$

Here, $E_{t30,A}$ and $E_{t30,C}$ are the "resting potentials" of each electrode after 30 s, which can be extrapolated by the depolarization transient for a large depolarization time instead of the measured 30 s (compare Equations (1) and (2)).

The values of $E_{corr,A}$ and $E_{IR,A}$, as well as $E_{corr,C}$ and $E_{IR,C}$ are now numerically extrapolated data from the depolarization curves and subjectable to the transient analysis following Equations (1) and (2).

3.2 | System response to chloride ingress

Figures 6 and 7 show the development of the regularly logged corrosion current and corrosion potential. The system response of increasing cell currents and decreasing corrosion potentials is not only valid for the general period of chloride contamination (compare Figure 7); moreover, it yields a very sharp response onto the weekly repetition of chloride solution penetration (compare Figure 6).

The precise and quasi-spontaneous system response to chloride penetration demonstrates the significantly shortened time needed for corrosion initiation in contrast to uncracked concrete.[17–21]

3.3 | Transient analysis

In Figure 8, the development of the transient depolarization time constants RC_A and RC_C is shown. As mentioned earlier, the time constants provide a quantitative measure of electrode kinetics. Due to the incorporation of double layer capacity, the active electrode surface is implemented within these time constants as well. Time constant values indirectly depend on the charge-transfer kinetics and electrode surface accessibility. Analogously to the corrosion current and the corrosion potential, the time constants RC_A and RC_C are directly linked to the duration of chloride exposure. With values ranging from 20 to 40 s, the cathodic time constant is always higher than the anodic time constant with values from 7 to 20 s. This also indicates that in this case, the cathodic depolarization process is always more inert as more time is needed to reach a theoretical depolarized state. This is even more confirmed as the cathodic time constant increases with the end of chloride exposure as the concrete dries out and the water content needed for sufficient cathodic reaction decreases. The mean and standard deviation of both time constants significantly decrease with the onset of chloride exposure. As Equations (1) and (2) rely on ideal electric circuits, it is confirmed that the standard deviation decreases with increasing cell current.

The obtained absolute values of 7–40 s are in very good agreement with the values of Glass et al.[9], which vary from

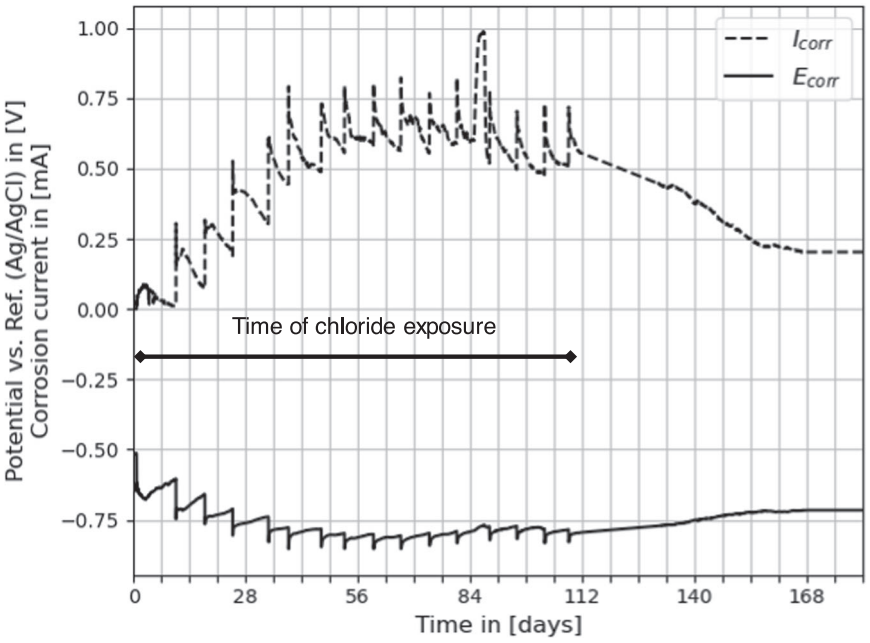

FIGURE 6 Development of a single, representative specimen. Precise system response onto the weekly driven chloride exposure

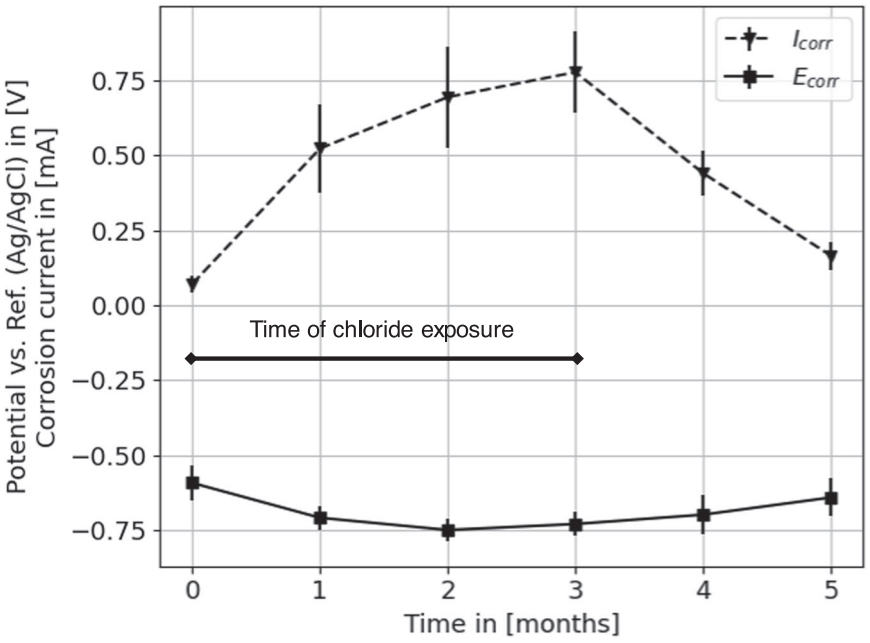

FIGURE 7 Development of the averaged corrosion current and corrosion potential during and after chloride exposure

7 to 65 s with active to negligible corrosion activity. Even though their equations rely on current density modeling and a different, varying specimen setup, transient modeling appears to converge on certain kinetic values regardless of the specimen and the experimental setup. Therefore, clearly, further studies of quantification of on-site depolarization transients are required.

The time constant RC, which is discussed above, consists of the product of charge-transfer resistance R_{CT} and the as yet unknown double-layer capacitance C_{DL}. At first glance, C_{DL} could easily be calculated from the quotient of time constant and polarization resistance. But as diffusion-controlled processes and the complex impact of microcell corrosion set in, once the current circuit is opened, the extrapolation of C_{DL} and the implicated electrode surface need further investigations.

Furthermore, the present double layer in cracked, reinforced concrete is not just partially disordered; its geometry has complex, three-dimensional structures, and the correlation of capacitance and surface is not linear when the capacitor is not coplanar.

As a consequence, the given capacitor needs to be replaced with a Warburg element to enable the quantification of diffusion-controlled processes within the

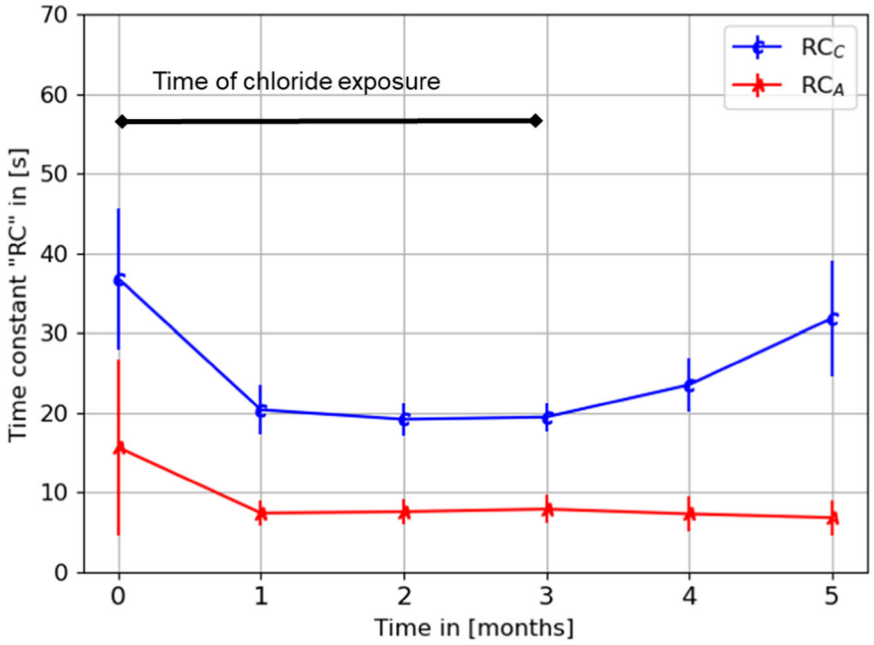

FIGURE 8 Transient depolarization time constants RC_A and RC_C during and after chloride exposure [Color figure can be viewed at wileyonlinelibrary.com]

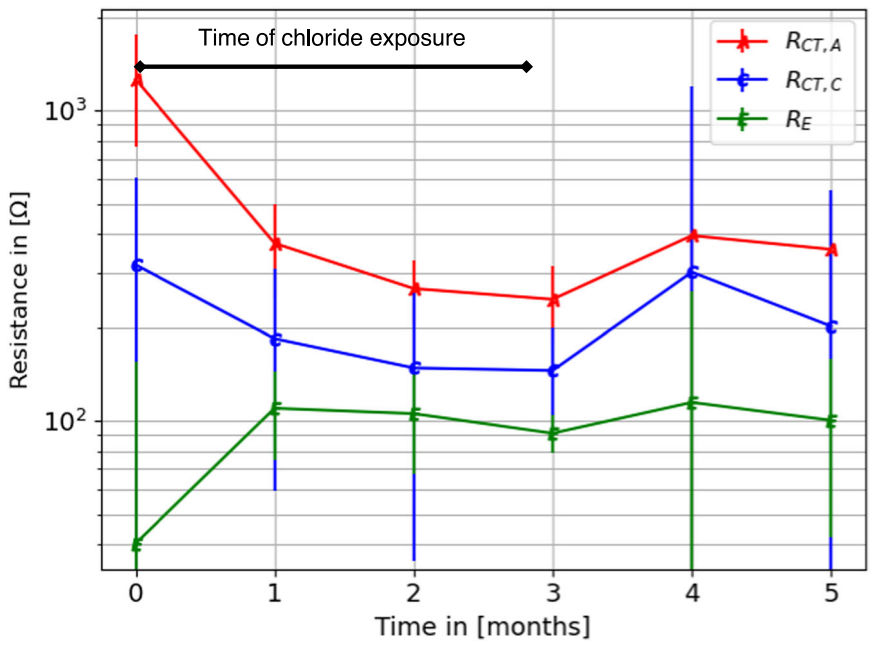

FIGURE 9 System resistances $R_{CT,A}$, $R_{CT,C}$, and R_E during and after chloride exposure [Color figure can be viewed at wileyonlinelibrary.com]

double layer.[22,23] A viable way to establish the proportional influence of diffusion on the depolarization criteria would be to establish a rather similar specimen setup, but with parametric variation of diffusion-controlling conditions during pre- and posttreatment.

As shown in Figure 9, the monitoring parameters polarization and electrolytic resistances proceed in reasonable accordance to chloride exposure, even though they are not measured but mathematically extrapolated from the measurement of 30 s depolarization. All three parameters appear to have rather small values in comparison to other studies of polarization resistances and need to be subjected to further and thus redundant investigations by linear polarization resistance measurements.[24,25]

4 | CONCLUSIONS

The present article deals with the results of a German research project exploring the measurability of chloride-induced corrosion mechanisms in cracked reinforced concrete. Here, high-frequency depolarization measurements were carried out and numerically analyzed based on the approaches reported by Glass et al.[9]

The following findings were obtained:

- The combination of gradient and transient analyses serves as a valuable, commonly adaptable, and time-saving tool for corrosion monitoring. As the database of depolarization transient time constants for experimental and on-site structures grows in the future, this measure can support building preservation with respect to corrosion activity.
- Corrosion current and corrosion potentials show sensitivity to chloride exposure in cracked reinforced concrete beams. This sensitivity is reflected in the results of the aforementioned numerically derived parameters.
- The limitations of the presented method were discussed. In particular, the lack of implementation of diffusion-controlling features should be investigated in further research.

In future studies, electrochemical investigations focused on transverse cracks initiated by bending and separation will be carried out. In particular, the focus will be on linear polarization resistances and specific electrolytic resistance.

ACKNOWLEDGMENTS

This study was supported by the Federal Ministry for Economic Affairs and Energy and sponsored by Projektträger Jülich (PtJ). Open Access funding enabled and organized by Projekt DEAL.

CONFLICT OF INTEREST

The authors declare that there are no conflict of interest.

AUTHOR CONTRIBUTIONS

Christoph Zausinger was involved in conceptualization of this study, investigations, and writing of the paper. The original draft and project management has been driven by Christoph Gehlen. Kai Osterminski was involved in review and editing of the paper.

DATA AVAILABILITY STATEMENT

The data that support the findings of this study are available from the corresponding author upon reasonable request.

ORCID

Christoph Zausinger https://orcid.org/0000-0001-7254-4136

REFERENCES

[1] M. Brem, *Ph.D. Thesis*, ETH Zurich (Switzerland) **2004**.
[2] S. Kessler, *Ph.D. Thesis*, TU Munich (Germany) **2015**.
[3] J. Warkus, M. Raupach, *Mater. Corros.* **2010**, *61*, 494.
[4] S. Jäggi, *Ph.D. Thesis*, ETH Zurich (Switzerland) **2001**.
[5] F. Hiemer, D. Jakob, S. Kessler, C. Gehlen, *Mater. Corros.* **2018**, *69*, 1526.
[6] J. Ožbolt, F. Orsanić, G. Balabanić, *Mater. Corros.* **2016**, *67*, 542.
[7] H. S. Isaacs, J. H. Cho, *Corros. Sci.* **1993**, *35*, 97.
[8] N. Birbilis, L. J. Holloway, *Cem. Concr. Compos.* **2007**, *29*, 330.
[9] G. K. Glass, C. L. Page, N. R. Short, J.-Z. Zhang, *Corros. Sci.* **1997**, *39*, 1657.
[10] C. Andrade, C. Alonso, J. Gulikers, R. Polder, R. Cigna, Ø. Vennesland, M. Salta, A. Raharininaivo, B. Elsener, *Mater. Struct.* **2004**, *37*, 623.
[11] T.-F. Mayer, C. Dauberschmidt, B. Bruns, T. Eichler, U. Wiens, J. Mietz, C. Gehlen, G. Ebell, G. Gerhard, K. Osterminski, *Bautechnik* **2020**, *97*, 2.
[12] F. Hiemer, F. Wich, C. Gehlen, S. Kessler, T. Mayer, *Sonderheft Messtechnik im Bauwesen*, Ernst & Sohn Special, Munich,**2018**, p. 1526.
[13] U. Feliu, J. A. Gonzalez, S. Feliu, *J. Appl. Electrochem.* **2005**, *35*, 429.
[14] U. M. Angst, M. R. Geiker, M. C. Alonso, R. Polder, O. Burkan Isgor, B. Elsener, H. Wong, A. Michel, K. Hornbostel, C. Gehlen, R. François, M. Sanchez, M. Criado, H. Sørensen, C. Hansson, R. Pillai, S. Mundra, J. Gulikers, M. Raupach, J. Pacheco, A. Sagüés, *Mater. Struct.* **2019**, *52*, 88.
[15] K. Osterminski, *Ph.D. Thesis*, TU Munich (Germany) 2013.
[16] M. Raupach, *Zur chloridinduzierten Makroelementkorrosion von Stahl in Beton*, DAfStb-Heft 433, Berlin, **1999**.
[17] O. Gautefall, Ø. Vennesland, *Nordic Concr. Res.* **1983**, *2*, 17.
[18] N. S. Berke, M. P. Dallaire, M. C. Hicks, R. J. Hoopes, *Corrosion* **1993**, *49*, 934.
[19] P. Schiessl, M. Raupach, *ACI Mater. J.* **1997**, *94*, 56.
[20] R. François, G. Arliguie, *Mag. Concr. Res.* **1999**, *51*, 143.
[21] T. U. Mohammed, N. Otsuk, M. Hisada, T. Shibata, *J. Mater Civ. Eng.* **2001**, *13*, 194.
[22] A. A. Sagüés, S. C. Kranc, E. I. Moreno, *Electrochim. Acta* **1996**, *41*, 1239.
[23] A. A. Sagüés, S. C. Kranc, E. I. Moreno, *Corros. Sci.* **1995**, *37*, 1097.
[24] U. M. Angst, M. Büchler, *Concrete Repair, Rehabilitation and Retrofitting IV*, CRC Press, Boca Raton **2015**.
[25] P. V. Nygaard, M. R. Geiker, *Mater. Corros.* **2012**, *63*, 200.

How to cite this article: C. Zausinger, K. Osterminski, C. Gehlen, *Mater. Corros.* **2022**;73:932–939.
https://doi.org/10.1002/maco.202112839